Effect of Laser Remelting on Microstructure, Residual Stress, and Mechanical Property of Selective Laser Melting-Processed Ti-6Al-4V Alloy

Yiwa Luo, Yu Jiang, Jun Zhu, Jiguo Tu, and Shuqiang Jiao

Abstract Laser remelting is often used during selective laser melting (SLM) processes to restrain the residual stress and improve the mechanical strength of the products. However, researches regarding its effects on porous metals with trabecular or thin-walled structure are still quite lacking. Hereby, remelting treatments have been employed during the SLM processes of a porous Ti-6Al-4V alloy in this study and their influences on dimensional accuracy, microstructure, mechanical property, and residual stress were researched. The results indicate that remelting treatments can provide a stronger bonding condition for the cellular structure, and improve the yield strength and elastic modulus of the alloy. Rescanning with 75% energy density results in 33.5–38.0% reduction of residual stress. In terms of pore structure and morphology, the porosities of remelted specimens are 2–4% lower than that of single-scanned specimens. This inconsistency increases with the increase of sheet thickness. It is suggested that the rescan laser power should be turned down during the preparation of porous titanium with thick cell walls to ensure dimensional accuracy.

Keywords Ti-6Al-4V · Selective laser melting · Residual stress · Mechanical property

Y. Luo · J. Tu · S. Jiao (✉)
State Key Laboratory of Advanced Metallurgy, University of Science and Technology Beijing, Beijing 100083, People's Republic of China
e-mail: sjiao@ustb.edu.cn

Y. Jiang
The Department of Orthopedics, Peking University Third Hospital, Beijing 100191, People's Republic of China
e-mail: medicojoe@126.com

J. Zhu
Ningxia Deyun Titanium Co Ltd., Shizuishan, Ningxia 735000, People's Republic of China

TMS 2021 150th Annual Meeting & Exhibition Supplemental Proceedings,
The Minerals, Metals & Materials Series,
https://doi.org/10.1007/978-3-030-65261-6_8

Introduction

Selective laser melting (SLM) technique integrates advanced laser technology, CAD design, and powder metallurgy technology, which has great advantages in the preparation of porous materials with precise size and complex structure. Comparing with traditional methods, SLM technique can provide micro-porous structures with global morphological properties that are highly controlled through computer. However, metals processed by laser as heat source generally have great residual stress due to rapid heating and cooling [1]. Residual stress will lead to deformation and distortions, and in some extreme cases, can cause cracking [2]. The conventional stress relief annealing method can eliminate the residual stress of the implants, but if the material has been deformed or cracked, it can not be recovered by subsequent heat treatment. This problem can be solved by remelting treatment which reduce the residual stress of the material in situ SLM. Remelting could reduce the temperature gradient and avoide rapid melting/cooling of the alloy. Most of the related research focus on solid alloys; the research on porous parts was rare [3, 4].

The aim of the current study is to reduce the residual stress and improve the mechanical strength of alloys with porous structures during SLM, reducing production procedures, and ameliorate the rapid prototyping products. In this work, one of popular porous material, namely Ti-6Al-4V alloy, was chosen as the experimental material for SLM. The effect of remelting treatments is studied by characterizing on the samples' microstructure, mechanical properties, and residual stress.

Experimental

Materials

Table 1 shows the composition of Ti-6Al-4V-ELI powder with a particle size of 10–53 μm, used within this investigation. The oxygen content was 0.15 wt%, which is below the minimum requirement of the biomedical materials (0.20 wt%) [5].

Table 1 Chemical composition of Ti-6Al-4V powders wt%

Element	Ti	Al	V	Fe	O	N	C	H
Content	Bal	5.5–6.5	3.5–4.5	0.1	<0.15	<0.01	<0.03	<0.01

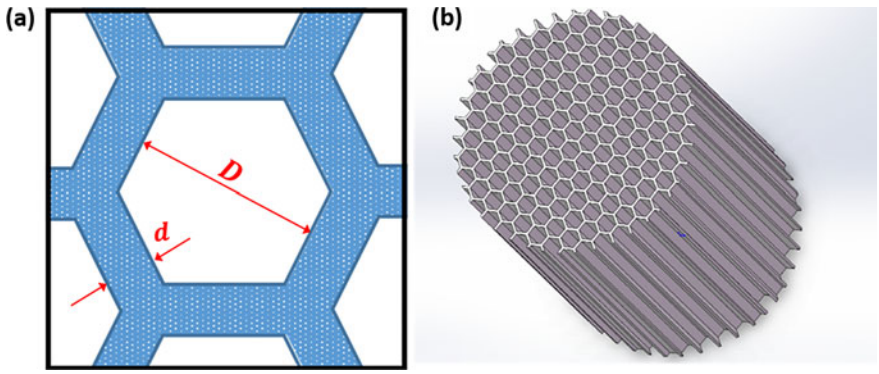

Fig. 1 Porous Ti-6Al-4V structure. **a** a unit cell, **b** the CAD model of the test sample. (Color figure online)

Fabrication of Porous Ti-6Al-4V by SLM 3D Printing

The unit cell used as the microarchitecture of the porous Ti alloy was honeycomb structure, which the porosity and pore size could be controlled by adjusting the CAD model parameter D and d (Fig. 1a). Porous structures with the same pore size ($D = 600\ \mu m$) and different thickness ($d = 100, 200, 300, 400$, and $500\ \mu m$) were designed and manufactured through SLM (EOS, M300, German). Cylindrical specimens with dimensions of $\varphi 10 \times 15\ mm^3$ and cubic specimens with the dimensions of $10 \times 10 \times 10\ mm^3$ were produced with their longitudinal axis perpendicular to the build plate (Fig. 1b).

The processing parameters used in this experiment were as follows: Power 240 W, scanning speed 0.8 m s^{-1}, layer thickness 30 μm, and scanning interval 50 μm. The specimens prepared via the above-mentioned process parameters were referred to *C-AM*. The other series of specimens were scanned again by double laser system immediately after each layer had experienced laser melting. The laser power and the scanning speed of the second scan in this experiment were set as 180 W and 0.5 m s^{-1}, respectively, which provided 75% of the energy density of the first scan.

Material Characterization

The cell wall and fracture morphology of the porous Ti-6Al-4V alloy were characterized employing a metalloscopy (Leica, Leica-DM4M, German) and field emission SEM (Carl Zeiss, Zeiss-EVO18, German). The metallographic photos of the specimens were analyzed via Image-Pro Plus software to measure the pore size.

Static uniaxial compression was carried out using a universal testing machine (XinSanSi, CMT4305, China) at room temperature following the standard of ASTM

E9-09. Average values are derived from the mean of five specimens for each Ti-6Al-4V alloy with a particular sheet thickness. Cylindrical specimens with a diameter of 10 mm and height of 15 mm were used for axial compression test, which the load was applied to the top of the cylinder. The cubic specimens with the dimensions of $10 \times 10 \times 10\ mm^3$ were used for radial compression test, which the load was applied to the cell walls.

A nano-indenter (MNT, N2100, America) was employed to measure the residual stress of titanium alloy with different sheet thickness. The specimens were polished and measured with a fixed load (1 mN). The measurement range of each sample was 3×3 lattice with the spacing of 10 μm between each indentation. Then calculated the residual stress of each sample by Suresh mode1 [6].

Results and Discussion

Physical Structures of the Porous Ti-6Al-4V Alloys

Figure 2 show the porosities of the porous Ti-6Al-4V structures produced by SLM the actual pore sizes of SLM-manufactural specimens are generally smaller than that of CAD models (Fig. 2a). Moreover, the inconsistency increases with the increasing cell thickness. The deviation is 32 μm when the cell thickness is 100 μm and 102 μm when the cell thickness is 500 μm. The porosity of the specimens is in the range of 40.4–78.6% (Fig. 2b). As discussed above, the actual porosities of specimens C-AM and D-AM are smaller than that of CAD models, and the error of specimens D-AM is 2–4% larger.

Microstructures of cell walls from C-AM and D-AM is investigated and shown in Fig. 3. The microstructure of Ti-6Al-4V alloy is mainly α acicular martensite because of the rapid cooling. The grain boundaries are clearly visible in the case of no double

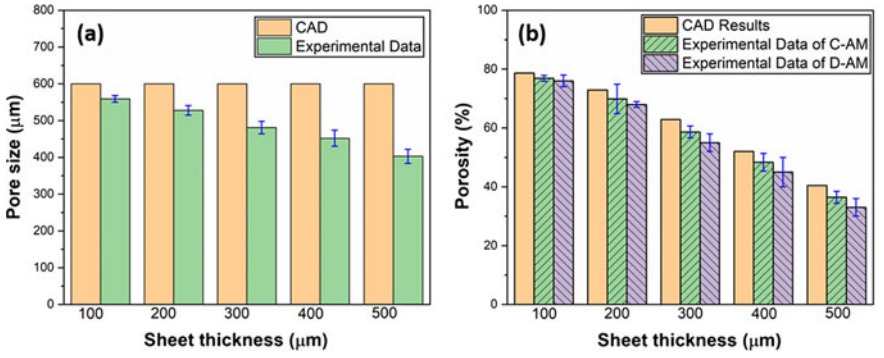

Fig. 2 **a** Comparison of the pore size of the SLM specimens and CAD models. **b** Porosities of the CAD models, C-AM and D-AM. (Color figure online)

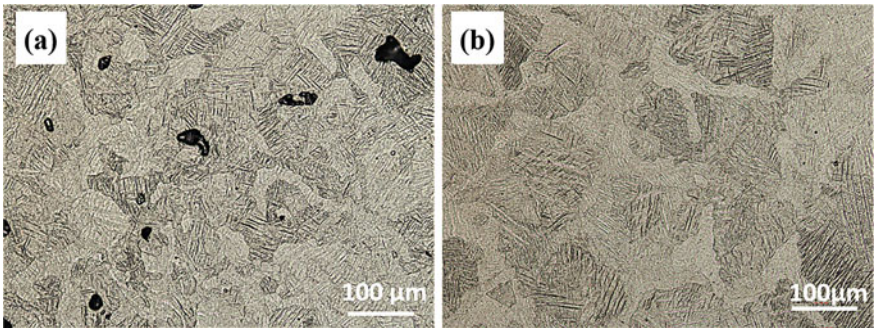

Fig. 3 SEM microtopography of the specimens fabricated by different processes. **a** C-AM200, **b** D-AM200. (Color figure online)

scanning. In contrast, the grain boundaries are unobvious due to the redistribution of chemical substances at high temperature after rescanning. The grains melt again when the laser rescans the powder layer, which leads to the epitaxial growth of the strengthened grains and martensite. The growth of martensite helps to improve the strength of Ti-6Al-4V alloy. However, martensite reduces the toughness of the alloy. Hence, the laser power of the second scan should be turned down suitably in order to avoid the brittleness of Ti-6Al-4V. The main defect of Ti-6Al-4V alloy melted by conventional technology is the irregular pores caused by unfused powder, and the defects are obviously reduced after rescanning.

Mechanical Properties and Deformation Mechanisms

The porosity of porous Ti-6Al-4V has a significant influence on its mechanical and biological properties. With the increase of the porosity, the strength decreases correspondingly. Uniaxial compression tests based on radial direction (RD) and axial direction (AD) have been conducted on the porous Ti-6Al-4V structures. Table 2

Table 2 Comparison of mechanical properties of the different types of porous Ti-6Al-4V

Sheet thickness	Yield strength (MPa)		Elastic modulus (GPa)		RD compressive strength (MPa)		AD compressive strength (MPa)	
	C-AM	D-AM	C-AM	D-AM	C-AM	D-AM	C-AM	D-AM
100	33.58	43.19	2.05	4.59	24.85	51.73	171.81	259.69
200	40.06	60.65	3.54	6.05	85.36	143.47	193.29	289.61
300	97.03	111.49	6.22	10.34	169.48	316.43	202.31	350.28
400	147.84	184.57	9.14	16.68	211.54	384.26	263.16	405.65
500	206.41	275.38	11.33	23.96	304.39	447.58	335.97	490.12

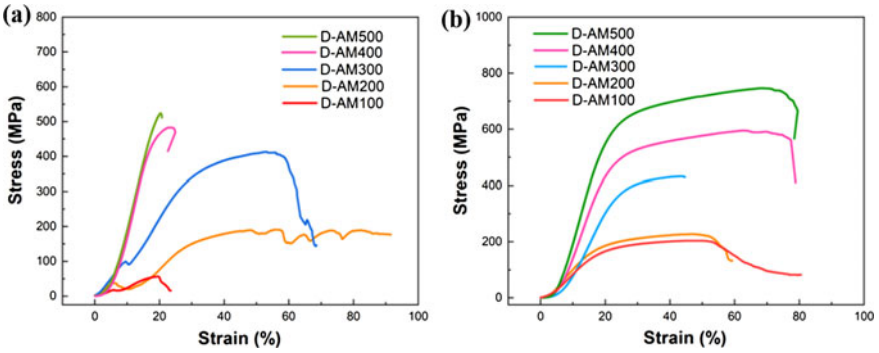

Fig. 4 Compressive stress/strain curves for the porous Ti-6Al-4V specimens. **a** radial direction, **b** axial direction. (Color figure online)

illustrates the details of the mechanical performance values of the single- and double-scanned samples. On account of the existence of pores, the yield strength and elastic modulus of porous Ti-6Al-4V are not as good as those of bulk alloy and decrease with the increase of porosity. The double-scanned structures reveal higher elastic modulus and better mechanical strength than the conventional porous structure. This is mainly attributed to the fact that remelting treatment could achieve a more uniform temperature and retain more solute segregation in the cell walls. The elastic modulus of porous Ti-6Al-4V prepared by new process in this work is in the range of 4.59 GPa-23.96 GPa.

Figure 4 depicted the RD and AD quasi-static stress/strain relationships of specimens D-AM during compression. The compressive stress/strain curve of porous titanium is usually consisted of three stages: linear elastic stage, platform stage, and densification stage [7]. From Fig. 4, the following characteristics can be concluded:

a. In the first stage of the stress/strain curve, the deformation of porous Ti-6Al-4V with different porosity presents linear elastic behavior in both radial and axial directions. The elastic modulus decreases with the decrease of sheet thickness.
b. The transition from the first stage to the second stage is smooth, and no obvious yield point can be observed on the stress/strain curve. It is suggested that the stress increases in a nonlinear way with the increase of compression stress.
c. In the second stage, the porous Ti-6Al-4V shows an obvious unsteady plateau stress in the radial direction, while in the axial direction, the plateau stress is more stationary. Moreover, specimens D-AM400 and D-AM500 are fractured directly under radial stress after yielding without plastic deformation, which is attributed to the reduction in plasticity based on the thickening of the cell walls.
d. In the third stage, the specimens with low porosities (D-AM300/D-AM400/D-AM500) are fractured when the compressive stress reaches the peak value. On contrast, porous Ti-6Al-4V with high porosities (D-AM100/D-AM200) enter the densification stage without obvious fracture.

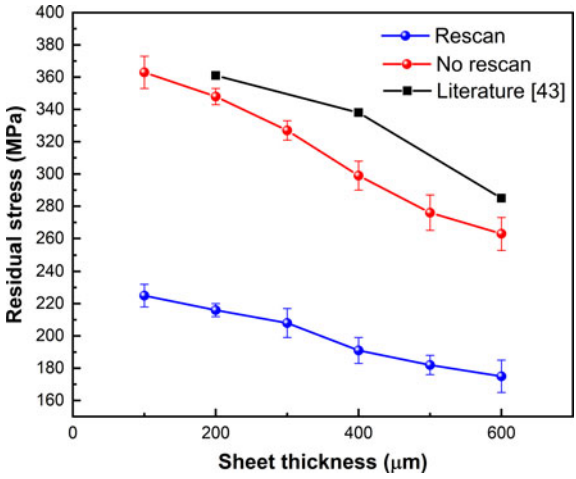

Fig. 5 Effect of rescanning on the residual stress of porous Ti-6Al-4V. (Color figure online)

In consequence, porous titanium with different sheet thickness has the same elastic deformation stage, but different plastic deformation stage.

Residual Stress

Figure 5 shows a relation between residual stress and sheet thickness. The residual stresses of the double-scanned specimens are 33.5–38.0% lower than that of the single-scanned specimens. A decrease in residual stress with increasing sheet thickness is consistent with the findings of Wang et al. [8] Ali et al. [9] reported that rescanning with 150% energy density resulted in 33.6% reduction in residual stress. However, the mechanical properties of the samples were reduced and failed prematurely. In the present study, the yield strength and elastic modulus of porous Ti-6Al-4V were improved through double scanning process with low power and slow speed.

Conclusions

In this work, 3D-printed porous Ti-6Al-4V with different cell wall thickness were produced through remelting treatment with 75% energy density. The porosities of remelted specimens are 2–4% lower than that of single-scanned specimens. The remelted structures reveal higher elastic modulus and better mechanical strength than the conventional porous structure. It is suggested that remelting treatment achieves a more uniform temperature and retains more solute segregation in the cell walls. The elastic modulus of porous Ti-6Al-4V prepared by remelting process in this

work is in the range of 4.59–23.96 GPa, and the density indexes are larger, which means the bonding conditions are stronger than those of single-scanned specimens. Rescanning with 75% energy density resulted in 33.5–38.0% reduction of residual stress. Moreover, the residual stress of porous Ti-6Al-4V decreases with increasing sheet thickness. This method could prove useful for decreasing residual stress in situ laser additive manufacturing while ensuring the dimensional accuracy of the thin-walled structure.

Acknowledgements This work was financially supported by the National Natural Science Foundation of China (Grant No. 51804012 and No. 51725401). The helpful comments, suggestions, and encouragement from editors and anonymous reviewers are gratefully acknowledged.

References

1. Strantza M, Ganeriwala RK, Clausen B, Phan TQ, Levine LE, Pagan D, King WE, Hodge NE, Brown DW (2018) Mater Lett 231:221
2. Roehling JD, Smith WL, Roehling TT, Vrancken B, Guss GM, McKeown JT, Hill MR, Matthews MJ (2019) Addit Manuf 28:228
3. Yu W, Sing SL, Chua CK, Tian X (2019) J Alloys Compd 792:574
4. Wei K, Lv M, Zeng X, Xiao Z, Huang G, Liu M, Deng J (2019) Mater Charact 150:67
5. Yan XC, Li Q, Yin S, Chen ZY, Jenkins R, Chen CY, Wang J, Ma WY, Bolot R, Lupoi R, Ren ZM, Liao HL, Liu M (2019) J Alloys Compd 782:209
6. Suresh S, Giannakopoulos AE (1998) Acta Mater 46:5755
7. Bobbert FSL, Lietaert K, Eftekhari AA, Pouran B, Ahmadi SM, Weinans H, Zadpoor AA (2017) Acta Biomater 53:572
8. Wang JF, Yuan JT, Wang ZH, Zhang B, Liu JX (2019) Laser Tech 43:411
9. Ali H, Ghadbeigi H, Mumtaz K (2018) Mater Sci Eng, A 712:175